



## Noncolinear optical parametric oscillator for broadband nanosecond pulse-burst CARS diagnostics in gases

ELIJAH R. JANS,<sup>1</sup>  DARRELL J. ARMSTRONG,<sup>1</sup> ARLEE V. SMITH,<sup>2</sup> AND SEAN P. KEARNEY<sup>1,\*</sup>

<sup>1</sup>Sandia National Laboratories, Albuquerque, New Mexico 87185, USA

<sup>2</sup>AS-Photonics, LLC, 6916 Montgomery Blvd. NE, Suite B8, Albuquerque, New Mexico 87109, USA

\*Corresponding author: [spkearn@sandia.gov](mailto:spkearn@sandia.gov)

Received 4 February 2022; revised 23 February 2022; accepted 23 February 2022; posted 1 March 2022; published 31 March 2022

**Demonstration of broadband nanosecond coherent anti-Stokes Raman scattering (CARS) using a burst-mode-pumped noncolinear optical parametric oscillator (NOPO) has been achieved at a pulse repetition rate of 40 kHz. The NOPO is pumped with the 355-nm output of a burst-mode Nd:YAG laser at 50 mJ/pulse for 45 pulses and produces an output centered near 607 nm, with a bandwidth of 370 cm<sup>-1</sup> at energies of 5 mJ/pulse. A planar BOXCARS phase matching scheme uses the broadband NOPO output as the Stokes beam and the narrowband 532-nm burst-mode output for the two CARS pump beams for single-laser-shot nitrogen thermometry in near adiabatic H<sub>2</sub>/air flames at temperatures up to 2200 K.**

<https://doi.org/10.1364/OL.455526>

Burst-mode laser diagnostics [1–3] for gas-phase systems are undergoing rapid development as applications in hypersonics and explosive systems experience renewed interest. By overdriving a Nd:YAG gain medium at low overall duty cycle, bursts of hundreds [4] or even thousands of laser pulses [5] are now available at repetition rates that can exceed 1 MHz, overcoming the data rate limitations associated with thermal management of repetitively pulsed lasers. Recent burst-mode diagnostic applications include velocimetry [6], Raman thermometry [7], and soot measurement via laser-induced incandescence [8]. Chemically specific measurements via planar laser-induced fluorescence (PLIF) [9,10] are additionally facilitated by burst-mode pumping of solid-state optical parametric oscillators and adaptation of DPSS-pumped dye lasers [11] for generation of tunable laser radiation at high repetition rates.

Coherent anti-Stokes Raman scattering (CARS) is a superior high-temperature gas-phase thermometer that has very recently been demonstrated using burst-mode lasers [2,12,13]. Fourier-transform limits for the 100–150 cm<sup>-1</sup> Stokes bandwidths required for CARS thermometry in flames impose a ~100-fs coherence time, and femtosecond pump and Stokes pulses provide a nearly ideal, transform-limited, low-noise Raman preparation [14]. Smyzer *et al.* [13] demonstrated a ~270-fs burst-mode source for MHz-rate CARS in room-temperature N<sub>2</sub>. While promising, key technical challenges remain to increase femtosecond pulse energies and bandwidths before the method

can be applied at high temperatures. Picosecond burst-mode operation [15] enables efficient solid-state optical parametric generation and subsequent parametric amplification to generate the required tunable, high-bandwidth Stokes source for CARS thermometry [2,12]. Long-duration picosecond and nanosecond pulses deliver broad spectral bandwidths by operating far from the transform limit. These pulses are characterized by stochastic, femtosecond-duration events in an essentially chaotic laser pulse, and this noise propagates into the resulting single-laser-shot CARS spectra. Despite this limitation, nanosecond laser pulses have been routinely applied for gas-phase CARS thermometry with good precision in the 3–5% range [16–18]. The single-shot noise is mitigated by time averaging over the long ~10-ns pulse duration, which is of the order of 100 Raman lifetimes in gas-phase N<sub>2</sub>. The 50- to 100-ps pulses employed for burst-mode CARS represent just a single Raman lifetime; time averaging is minimized, and CARS spectra display elevated noise that necessitates single-shot monitoring of the Stokes spectrum. Picosecond CARS additionally lies between the continuous-wave and impulsive limits represented by nanosecond and transform-limited femtosecond pulses, which may lead to additional uncertainties arising from the dependence of the CARS spectral shapes on the time-domain structure of the laser pulses and associated pulse delays.

The objective of this work is demonstration of burst-mode CARS thermometry using nanosecond laser pulses, which take advantage of the effectively CW nature of the ns-CARS processes and time-averaging of the Stokes source noise. We have constructed a broadband, burst-mode-pumped OPO, which is widely tunable throughout the visible spectrum and can deliver up to 5 mJ/pulse and full width at half maximum (FWHM) bandwidths of several hundred cm<sup>-1</sup> when pumped by 10-ns pulses at 355 nm from a burst-mode Nd:YAG laser.

The burst-mode-pumped OPO uses a noncollinear geometry to produce output beams with large spectral bandwidths [19]. The noncollinear geometry has been widely used in noncollinear optical parametric amplifiers (NOPA) for generating broad bandwidths, especially for fs pulse generation, over the last several decades [20]. Generation of bandwidths up to 100 nm using ns NOPO have also been demonstrated [21]. To first order, the bandwidth for parametric amplification is the inverse of the temporal walk off between the signal and idler waves due to the differing

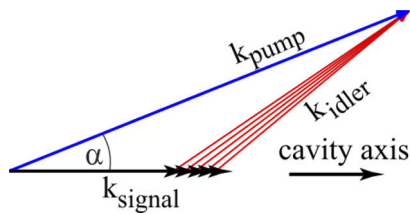


**Fig. 1.** Phase matching diagram for noncollinearly pumped OPO. The signal beam is parallel to the OPO cavity axis; the pump is tilted by angle  $\alpha$  from the cavity axis; the idler beam is angle dispersed to close the  $k$ -vector triangle. With the right value of  $\alpha$ , the group velocities of the signal and idler parallel to the cavity axis are equal and the bandwidth is maximized.

group velocities. If the group velocities can be made equal, the bandwidth is then limited by the second-order effects arising from group velocity dispersion. For  $N_2$  CARS, the spectra of the signal and idler beams are nominally centered near 607 nm and 855 nm, such that the idler has a higher group velocity than its partner signal wave. The effective group velocity of the idler wave can be slowed by tilting the beam as shown in the phase matching scheme of Fig. 1. The signal wave is resonant in the OPO cavity so its wave vector,  $k$ , must be parallel the cavity axis. By tilting the 355-nm pump beam relative to the cavity axis, the  $k$ -vector of the idler beam must also tilt to achieve phase matching. With the right choice of pump angle, the component of the idler group velocity along cavity (signal) axis will match the signal group velocity, maximizing the bandwidth of both OPO beams. To a first-order approximation, the frequency bandwidth,  $\Delta\nu$ , that may be expected from an OPO, assuming low gain, and a frequency-narrow minimally depleted pump is given by

$$\Delta\omega = \frac{1}{l_c |n_{gs} - n_{gi}|}, \quad (1)$$

where  $l_c$  is the crystal length,  $c$  is the speed of light, and  $n_{gs}$  and  $n_{gi}$  are the group velocities indices of the signal and idler beams, respectively [19]. For type-I parametric generation in BBO, with o-polarized signal and idler beams and an e-polarized pump beam, the crystal group velocity matching is achieved with a pump beam  $k$ -vector tilt of  $4.1^\circ$  relative to the cavity axis. The Poynting vector of the e-polarized 355-nm beam tilts by  $4.35^\circ$  relative to its  $k$ -vector due to birefringent walk off. Correct choice of the sign of the pump beam tilt relative to the cavity axis leads to a power flow (Poynting vector) of the pump light that is nearly parallel to that of the signal beam. Ideally, the idler beam is angle dispersed, as shown in the  $k$ -vector diagram, while the signal beam is not. In practice, the large diameter and single pass of the pump beam (as employed here) results in some angular dispersion of the signal beam as well.

The experimental setup for the CARS system, including the burst-mode-pumped NOPO, is shown in Fig. 2(a). A burst-mode Nd:YAG laser (Spectral Energies “Quasimodo”) provided both 532- and 355-nm pulses at 40-kHz pulse repetition rate. The laser was operated with a pulse width of 10 ns in the 1064-nm fundamental with a total burst duration of 1.5 ms. The NOPO was pumped at 355 nm and  $\sim 55$  mJ/pulse for 45-pulse burst and the diameter of the 355-nm NOPO pump beam was 3 mm with a flat-top intensity profile. A 90-mm-long OPO cavity was formed by two flat mirrors mounted on a rotary stage, with an intra-cavity pump mirror and Type-I  $\beta$ -barium-borate (BBO) crystal both mounted on platforms independent from the

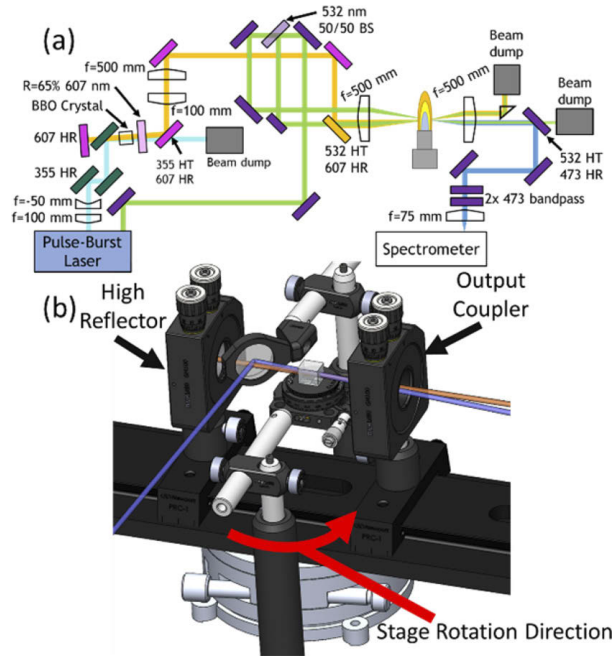


**Fig. 2.** (a) Experimental schematic of noncollinear optical parametric oscillator and CARS setup and (b) detailed view of NOPO design.

cavity. In this manner, the OPO cavity axis could be independently rotated with respect to the input 355-nm pump beam and the BBO crystal. A detailed depiction of the NOPO is shown in Fig. 2(b). Typical tilt angles of the cavity were  $3\text{--}5^\circ$  with the output bandwidth increasing with increasing tilt. For all measurements made in this paper, the cavity tilt was  $\sim 5^\circ$ . The uncoated BBO crystal was 10 mm  $\times$  10 mm across its face, 12 mm in length, and was cut with its optical axis at  $32.8^\circ$  to the crystal face. The signal-resonant cavity was composed of a high reflector for wavelengths  $\lambda = 598\text{--}610$  nm and an output coupler with  $R = 65\%$  for  $\lambda = 598\text{--}610$  nm and high transmission at  $\lambda = 355$  nm. The OPO was initially aligned with the pump axis parallel to the cavity axis in a typical collinear phase-matched OPO configuration. The cavity was then tilted gradually while observing the output spectrum of the OPO signal beam and rotating the angle of the BBO crystal to keep the center frequency of the signal wave at the desired position for  $N_2$  CARS.

Planar BOXCARS phase matching [22] was employed with the 532-nm from the burst-mode source split 50/50 to form two CARS pump beams, and the broadband output from the NOPO was used for the Stokes beam. The beams were crossed over a near-adiabatic  $H_2$ /air flat flame stabilized on a Hencken burner with a 5-cm  $\times$  5-cm square format, and the CARS probe volume was positioned 1 cm above the burner face. Pulse energies were 40 mJ in each of the CARS pump beams and 5 mJ in the Stokes pulses. The CARS signal was separated from the probe beam using several dichroic 473-nm high reflectors and two bandpass filters centered at 470 nm with a 20-nm FWHM. A 0.5-meter spectrometer (Princeton Instruments SpectraPro HRS-500) with a grating of 1800 l/mm dispersed the CARS signal onto an electron-multiplying (EM) CCD camera (Princeton Instruments Pro-EM-HS 1024). This EM-CCD enabled fast, 40-kHz acquisition of spectra by vertically shifting charge on each successive laser shot and using the entire 1024- $\times$  1024-pixel

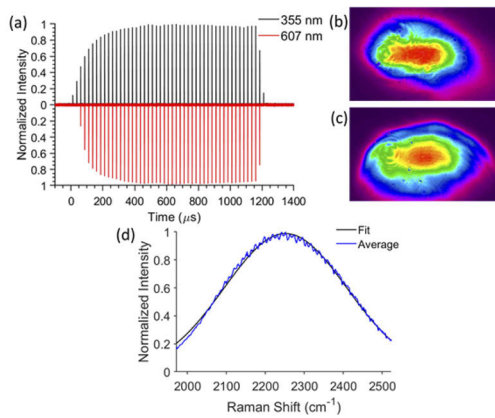


**Fig. 3.** (a) Relative intensities of the 355-nm and 607-nm beams at 40-kHz pulse repetition rate. Beam profiles from the NOPO (b) just after the OPO cavity and (c) 3 meters from the OPO cavity; and (d) nonresonant background taken in argon for an average of 15 bursts with a Gaussian fit for an inferred FWHM =  $370\text{ cm}^{-1}$ .

chip, and an adjacent 1024-pixel square masked area, to store all 45 single-laser-shot CARS spectra acquired during the burst prior to sensor readout. This type of camera has previously been demonstrated for burst-mode CARS at 100-kHz rates [2, 12] and for spontaneous-Raman scattering at 10 kHz [7]. A CARS interaction length of 17 mm, where 90% of the total CARS signal is generated, was determined by propagating a glass coverslip through the beam crossing.

Burst profiles for both the 355-nm pump (black) and 607-nm NOPO output (red) are shown in Fig. 3(a), where pulse uniformity of the NOPO for the short 45-pulse burst is generally observed to be excellent. Figure 3(b) shows the beam profile for the entire burst of the NOPO signal beam, measured just outside the OPO cavity, while Fig. 3(c) shows the beam profile at 3 m from the OPO, right before the measurement volume. The nonresonant background (NRB) CARS spectrum taken in argon and averaged over 15 45-pulse, 40-kHz bursts is shown in Fig. 3(d). The  $370\text{-cm}^{-1}$ -wide NRB spectrum represents a significant bandwidth reduction from the  $540\text{-cm}^{-1}$  FWHM bandwidth supplied by the NOPO, which is likely a result of the angular dispersion (spatial chirp) of the signal beam. As the CARS pump beams cross the focused Stokes profile, the overlap of the pumps encounters only the bandwidth within the Stokes beam center. This bandwidth is still more than what is typically used in ns CARS measurements, which is around  $150\text{ cm}^{-1}$  [23], and is sufficient for temperatures around 2000 K. Reduced angular dispersion in the NOPO output may be achieved via retroreflection of the 355-nm pump beam. Burst to burst, the CARS NRB had a center frequency variation of  $30\text{ cm}^{-1}$  (8%) and had a bandwidth variation of  $18\text{ cm}^{-1}$  (4.8%) over the 15 bursts observed.

Typical single-laser-shot  $\text{N}_2$  CARS spectra from the near-adiabatic  $\text{H}_2$ -air flame for equivalence ratios of  $f=0.52$ – $0.86$  are shown in Figs. 4(a)–4(d). Good single-shot signal-to-noise was observed over a wide range of flame temperatures, even with a relatively modest 5-mJ/pulse Stokes source energy. Gas temperatures were inferred from the CARS measurements using a least-squares fit to a library of spectra generated by the Sandia CARSFT code [24]. The noise in these single-shot CARS spectra is largely dominated by NOPO photon statistics. The

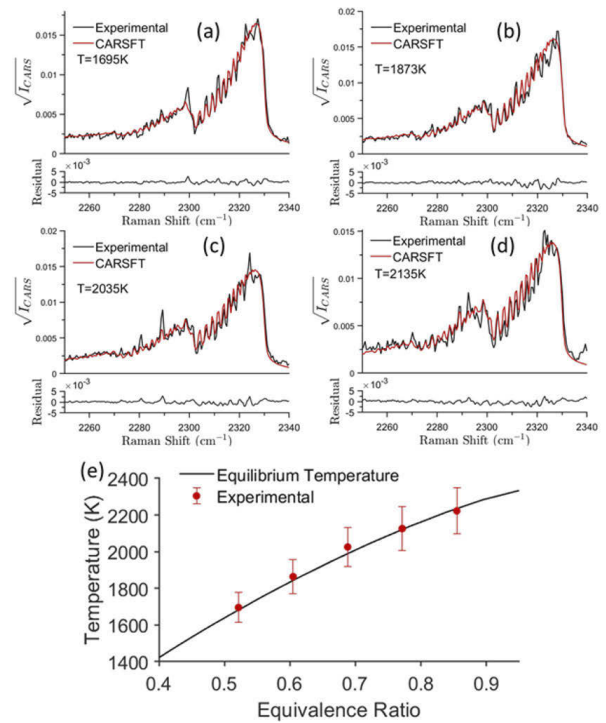


**Fig. 4.** Single-shot CARS signal from a 40-kHz pulse repetition rate burst in a Hencken burner flame fit with CARSFT for equivalence ratios of (a)  $\phi=0.52$ , (b)  $\phi=0.61$ , (c)  $\phi=0.77$ , and (d)  $\phi=0.77$ ; (e) CARS temperature inferred from single-shot data for 400 shots using five different equivalence ratios from a near-adiabatic  $\text{H}_2$ /air Hencken burner flame.

burst-mode laser used in this work is expected to exhibit near-transform-limited performance, so that pump laser statistics are not a significant contributor to the observed CARS noise. In principle, the Stokes source noise may be reduced by increasing the NOPO oscillator cavity length from  $\sim 9$  cm to 30 cm or more, which is typical of nanosecond broadband dye-laser systems used for gas-phase CARS. The longer cavity reduces longitudinal mode spacing, thereby increasing the number of modes interacting with a given Raman resonance [25]. Use of a longer NOPO cavity will result in higher pump energy at oscillation thresholds and reduced NOPO power, which may be overcome by adding parametric amplifiers to the Stokes source design.

The inferred temperature for five different equivalence ratios from  $\phi=0.52$  to  $0.86$  is shown in Fig. 4(e). The orange circles represent the mean temperature from 400 single-laser-shot realizations, while the error bars indicate the corresponding standard deviation in the temperature measurements. The observed single-shot measurement precision (one standard deviation) was 4.9% of the mean temperature at  $T=1696\text{ K}$  to 5.7% of mean at  $T=2126\text{ K}$ . Uncertainties in gas flow rates were accounted for by shifting the equivalence ratio axis in Fig. 4(e) by 0.105 for a best match agreement of the measured temperature curve to calculated adiabatic flame temperatures, after which mean CARS-measured temperatures were within 1.85% of the calculated values. The observed measurement precision was degraded by  $\sim 1.6$ – $2\times$  relative to the nominally 3% levels attained with 10-Hz nanosecond vibrational CARS under ideal laboratory conditions [16, 26] using single-mode pump lasers, but was

comparable to some vibrational CARS measurements using multimode pump lasers [26] as well as some early reports of pure-rotational nanosecond CARS thermometry in flames [27]. The observed precision of flame temperatures using the burst-mode-pumped ns-NOPO was close to the values reported in [12] obtained with a burst-mode pumped picosecond OPG with shot-to-shot NRB normalization to correct for Stokes spectral noise. Comparing the two demonstrations of pulse-burst CARS measurements, the nanosecond NOPO system has several advantages, such as less complexity, lower inherent noise, and the potential to approach the precision seen in 10-Hz nanosecond CARS instruments.

In summary, we have demonstrated a broadband burst-mode-pumped NOPO for single-laser-shot 40-kHz CARS thermometry. Relative to recent picosecond burst-mode CARS measurements [12], nanosecond laser pulses remove uncertainties associated with the time-dependent nature of the picosecond CARS process and result in lower single-laser-shot noise as a result of time averaging, mitigating the need for shot-to-shot Stokes spectrum corrections. Stokes bandwidths as high as  $370\text{ cm}^{-1}$  were coupled to the CARS process. Single-laser-shot thermometry from fits to the  $\text{N}_2$  Q-branch spectrum at flame temperatures from 1700 K to 2200 K have been observed with a precision of 4.9–5.7%. This measurement precision is comparable to recent picosecond burst-mode CARS measurements with shot-to-shot Stokes spectrum corrections, but the burst-mode ns NOPO CARS data do not require shot-to-shot NRB corrections. The current system has a sensitivity of approximately 50 K and an upper measurement limit of 2500 K. Noise in these single-shot spectra is dominated by NOPO photon statistics, which can be improved by increasing the oscillator cavity length and addition of noncolinear optical parametric amplifier (OPA) stages to compensate for the expected loss of NOPO energy. The measurements reported here demonstrate feasibility of nanosecond burst-mode CARS thermometry at 40-kHz extension to 100-kHz [2,12] or higher rates is straightforward with a more energetic pump laser.

**Funding.** Sandia National Laboratories; Laboratory Directed Research and Development; U.S. Department of Energy's National Nuclear Security Administration (DE-NA0003525).

**Acknowledgment.** Sandia National Laboratories is a multi-mission laboratory managed and operated by National Technology and Engineering Solutions of Sandia, LLC., a wholly owned subsidiary of Honeywell International, Inc., for the U.S. Department of Energy's National Nuclear Security Administration under contract DE-NA0003525.

**Disclosures.** The authors declare no conflicts of interest.

**Data availability.** Data underlying the results presented in this paper are not publicly available at this time but may be obtained from the authors upon reasonable request.

## REFERENCES

1. B. Thurow, N. Jiang, and W. Lempert, *Meas. Sci. Technol.* **24**, 012002 (2013).
2. S. Roy, P. S. Hsu, N. Jiang, M. N. Slipchenko, and J. R. Gord, *Opt. Lett.* **40**, 5125 (2015).
3. P. Wu, W. L. Lempert, and R. B. Miles, *AIAA J.* **38**, 672 (2000).
4. M. N. Slipchenko, T. R. Meyer, and S. Roy, *Proc. Combust. Inst.* **38**, 1533 (2021).
5. M. N. Slipchenko, J. D. Miller, S. Roy, T. R. Meyer, J. G. Mance, and J. R. Gord, *Opt. Lett.* **39**, 4735 (2014).
6. S. Beresh, S. Kearney, J. Wagner, D. Guildenbecher, J. Henfling, R. Spillers, B. Pruet, N. Jiang, M. Slipchenko, and J. Mance, *Meas. Sci. Technol.* **26**, 095305 (2015).
7. C. Winters, T. Haller, S. Kearney, P. Varghese, K. Lynch, K. Daniel, and J. Wagner, *Opt. Lett.* **46**, 2160 (2021).
8. T. R. Meyer, B. R. Halls, N. Jiang, M. N. Slipchenko, S. Roy, and J. R. Gord, *Opt. Express* **24**, 29547 (2016).
9. N. Jiang, M. Webster, W. R. Lempert, J. D. Miller, T. R. Meyer, C. B. Ivey, and P. M. Danehy, *Appl. Opt.* **50**, A20 (2011).
10. J. D. Miller, M. Slipchenko, T. R. Meyer, N. Jiang, W. R. Lempert, and J. R. Gord, *Opt. Lett.* **34**, 1309 (2009).
11. S. D. Hammack, C. D. Carter, A. W. Skiba, C. A. Fugger, J. J. Felver, J. D. Miller, J. R. Gord, and T. Lee, *Opt. Lett.* **43**, 1115 (2018).
12. D. K. Lauriola, P. S. Hsu, N. Jiang, M. N. Slipchenko, T. R. Meyer, and S. Roy, *Opt. Lett.* **46**, 5489 (2021).
13. M. E. Smyser, E. L. Braun, V. Athmanathan, M. N. Slipchenko, S. Roy, and T. R. Meyer, *Opt. Lett.* **45**, 5933 (2020).
14. R. P. Lucht, S. Roy, T. R. Meyer, and J. R. Gord, *Appl. Phys. Lett.* **89**, 251112 (2006).
15. S. Roy, J. D. Miller, M. N. Slipchenko, P. S. Hsu, J. G. Mance, T. R. Meyer, and J. R. Gord, *Opt. Lett.* **39**, 6462 (2014).
16. T. Seeger and A. Leipertz, *Appl. Opt.* **35**, 2665 (1996).
17. P. Snowden, S. Skippon, and P. Ewart, *Appl. Opt.* **30**, 1008 (1991).
18. P.-E. Bengtsson, M. Aldén, S. Kröll, and D. Nilsson, *Combust. Flame* **82**, 199 (1990).
19. A. V. Smith, *Crystal Nonlinear Optics: With SNLO examples*, 2nd ed. (AS-Photonics, 2018).
20. G. Gale, M. Cavallari, and F. Hache, *J. Opt. Soc. Am. B* **15**, 702 (1998).
21. J. Wang, M. H. Dunn, and C. F. Rae, *Opt. Lett.* **22**, 763 (1997).
22. A. C. Eckbreth, *Appl. Phys. Lett.* **32**, 421 (1978).
23. S. Roy, J. R. Gord, and A. K. Patnaik, *Prog. Energy Combust. Sci.* **36**, 280 (2010).
24. R. Palmer, "The CARSFT computer code calculating coherent anti-stokes raman spectra: User and programmer information," Sandia National Lab.(SNL-CA), Livermore, CA (United States, (1989) <https://www.osti.gov/biblio/6399189>).
25. S. Kröll, M. Aldén, T. Bergliind, and R. J. Hall, *Appl. Opt.* **26**, 1068 (1987).
26. D. Snelling, G. Smallwood, R. Sawchuk, and T. Parameswaran, *Appl. Opt.* **26**, 99 (1987).
27. M. Aldén, P.-E. Bengtsson, H. Edner, S. Kröll, and D. Nilsson, *Appl. Opt.* **28**, 3206 (1989).